J Nanopart Res (2013) 15:1846
DOI 10.1007/s11051-013-1846-4

RESEARCH PAPER

Probing the structure of Fe nanoparticles in multiwall carbon nanotubes grown on a stainless steel substrate

L. Camilli · P. Castrucci · M. Scarselli · E. Gautron · S. Lefrant · M. De Crescenzi

Received: 17 May 2013 / Accepted: 8 July 2013

Abstract We investigated the local order in individual iron nanoparticles (NPs) embedded in carbon nanotubes (CNTs). The NPs directly come from the CNT growth on stainless steel without addition of external metal catalyst. The structural analysis has been obtained through nanoscale transmission extended electron energy loss fine structure (EXELFS) measurements above the iron $L_{2,3}$ edge. A theoretical simulation of the EXELFS features has been performed within the multiple scattering theory. By comparing the experimental data with the simulations, we found that pure γ-Fe and Fe_3C nanoparticles are the catalysts of the CNT synthesis on the stainless steel. Moreover, from the analysis of the fine details of the EXELFS oscillations, we also estimated the value of the fcc Fe NP lattice parameter to be $a = 3.61 \pm 0.03$ Å. This last finding suggests a high magnetic moment of the fcc Fe NPs.

L. Camilli · P. Castrucci (✉) · M. Scarselli · M. De Crescenzi
Dipartimento di Fisica and Unità CNISM, Università Roma Tor Vergata, Via della Ricerca Scientifica 1, 00133 Rome, Italy
e-mail: paola.castrucci@roma2.infn.it

E. Gautron · S. Lefrant
Institut des Matériaux Jean Rouxel (IMN), Université de Nantes, CNRS, 2 rue de la Houssinière, BP 32229, 44322 Nantes Cedex 3, France

Keywords Fcc iron · Extended electron energy loss fine structure (EXELFS) spectroscopy · Iron nanoparticles · Carbon nanotubes

Introduction

Face-centered cubic (fcc) bulk iron (the so called γ-Fe) phase is paramagnetic and stable at temperatures between 1,183 and 1,667 K (Massalski and Okamoto 1992). Nevertheless, the possibility to form iron fcc structures at room temperature has attracted much interest. This was in part stimulated by some calculations predicting, for bulk fcc iron with a lattice parameter, a, between 3.4 and 3.7 Å, a ferromagnetic behavior with atomic moments, for $a \geq 3.59$ Å, significantly enhanced ($\geq$2.5 μ_B/atom) if compared to the value in bulk body-centered cubic (bcc) iron (α-Fe) ($\sim$2.2 μ_B/atom) (Moruzzi et al. 1986; Bagayoko and Callaway 1983). This theoretical indication made the iron fcc structure appealing from the point of view of potential applications. To obtain such a γ-Fe phase, several attempts have been made: (i) alloying Fe with other elements such as Ni (like in stainless steel); (ii) epitaxially growing Fe ultra thin films on Cu (Shen et al. 1998) or Cu/Si (Gubbiotti et al. 1999) substrates; (iii) forming fcc Fe precipitates in Cu (Hines et al. 2009) or $Cu_{1-x}Au_x$ (Klein et al. 1991) matrix through heat treatments; (iv) synthesizing γ-Fe nanoparticles and nanowires on a carbon film (Ling et al. 2008,

Published online: 24 July 2013

2009); and (v) very recently embedding iron fcc nanoparticles in carbon nanotubes (CNT) (Lyubutin et al. 2012). These last studies are particularly appealing because (i) it is possible to grow highly oriented CNTs, leading to anisotropic magnetic response of the device (Lyubutin et al. 2012), and (ii) the surrounding CNT walls protect the metallic nanostructures from the action of ambient oxygen (Camilli et al. 2011). For these reasons, extensive investigations have been devoted to CNTs filled with ferromagnetic metals to be used as superdense magnetic recording (Li et al. 2000), as magnetic force microscope tips (Winkler et al. 2006), magnetic field sensors or nanocontainers for targeted drug delivery (Mönch et al. 2007). Different experimental approaches have been employed to fabricate metal-filled or partially filled CNTs: e.g., by means of capillarity (Borowiak-Palen et al. 2006), catalytic chemical vapor deposition (CVD) (Lyubutin et al. 2012), and chemical vapor deposition (He et al. 2011). As a matter of facts, iron nanoparticles filling the CNTs have been found to possess different nature, namely α-Fe, Fe_3C and/or γ-Fe, depending on the synthesis conditions. X-ray diffraction as well as electron diffraction performed in a transmission electron microscopy (TEM) apparatus are the most used techniques to study the structural properties of these nanoparticles. While XRD investigation provides information averaged on huge number of nanoparticles, electron diffraction has the advantage to give the structure of the individual nanostructures imaged by TEM. In this framework, a useful complementary experimental technique is the electron energy loss spectroscopy (EELS) and its associated extended electron energy loss fine structure (EXELFS) spectroscopy. This technique, like electron diffraction, has nanoscale spatial resolution, and also allows to perform a study of the chemical nature and local atomic ordering in the selected area exposed to the electron beam spot. In fact, within the limit of the dipole approximation, the EXELFS oscillations can be analyzed as the extended X-ray absorption fine structure (EXAFS) data (Stöhr 1988), thus allowing to determine the local atomic structure around the ionized atom, such as bond lengths and coordination number, and the dynamic disorder (i.e., the atomic thermal vibration around the equilibrium position). On the other hand, since the amount of inelastically scattered electrons drastically decreases with the increasing energy loss, giving rise to small peaks superimposed on a strongly decreasing background, only edges with energies lower than 1,000 eV can be easily recorded. This means that, in the case of iron, only the EXELFS oscillations around the $L_{2,3}$ edges (above 708 eV) can be investigated. The K edge (around 7,100 eV) is indeed too far in energy loss from the elastic peak thus exhibiting a very low inelastic cross section ($\sim \Delta E^{-4}$, where ΔE being the energy loss) (Auerhammer and Rez 1989). However, analyzing the EXELFS (as well as EXAFS) oscillations over the iron L edges is quite challenging because of substantial difficulties due to the spin–orbit splitting of the 2*p* state. Studies of EXAFS spectra performed on thin film of bcc iron around the Fe L edges have been already published (Kurde et al. 2007). In the case of nanoparticles, the rather low number of atoms makes this experiment a true challenge in terms of signal-to-noise ratio of the EXELFS spectra. In addition, the encapsulation of the nanoparticle inside the CNT walls further reduces the signal to be collected.

Here, we report on an EXELFS study with the aim at investigating the structure of the metal nanoparticles embedded in the CNTs that have catalyzed the CNT growth process. Our analysis of the experimental EXELFS oscillations ensured us on the γ-Fe phase nature of several nanoparticles imaged by TEM and allowed us to estimate the lattice parameter of the fcc iron structure to be around 3.61 Å. Noticeably, such a value of the γ-Fe phase lattice parameter makes them possible candidates to be ferromagnetic at room temperature and have atomic moment higher than that of bulk α-Fe. In addition, we were able to detect the presence of iron carbide nanoparticles, too.

Experimental details

The CNTs are synthesized by chemical vapor deposition from acetylene directly on AISI-316 stainless steel (Fe 70 %, Cr 18 %, and Ni 10 %). Once the stainless steel is heated up to 1,003 K, acetylene (200 sccm) is introduced in the chamber for 10 min in dynamic conditions, thus allowing the CNT growth. More details on the synthesis of iron-filled CNTs are described by Camilli et al. (2011). α-Fe microparticles, used as reference for the EXELFS measurements,

have been obtained from an iron powder (from R. P. Normapur) after reduction in H_2 at 973 K for 10 h followed by a subsequent rapid introduction in the TEM apparatus.

Iron-filled CNT samples for TEM experiments were prepared by scratching the synthesis product from the stainless steel surface directly on a holey carbon-coated TEM grid. Imaging and EXELFS data acquisition were performed with a cold FEG Hitachi HF2000 transmission electron microscope (TEM) equipped with a modified Gatan PEELS 666 spectrometer. All the EXELFS measurements were recorded in the same experimental conditions: accelerating voltage 100 kV, diffraction coupling mode, energy dispersion of 0.3 eV/channel, convergence angle 2.8 mrad, and collection angle 9.1 mrad. This collection angle was chosen very close to the so-called "magic angle" (7.8 mrad at 710 eV), so that spectra do not vary with sample orientation (Jouffrey et al. 2004).[1] Deconvolution was performed with PEELS Cambridge software (Fallon and Walsh 1996) to remove the instrument contribution and the plural scattering effects. TEM images were acquired before and after each electron energy loss spectroscopy (EELS) measurement to ensure that the area under investigation had not suffered any morphological change and/or damage that may arise from its long exposure to the high-energy electron beam. Various sizes of nanoparticles were successfully analyzed following this procedure. However, EXELFS spectra with satisfactory signal-to-noise ratio were quite challenging to obtain on individual small nanoparticles. This difficulty is mainly due to the low amount of atoms to detect. Moreover, near-edge EELS spectra were systematically recorded, with suitable energy range, to detect the presence of any feature of the Cr and Ni $L_{2,3}$ or O K edges. As far as Ni content regards, very few of the observed iron nanoparticles presented small traces of Ni. The present EXELFS analysis has been limited to those nanostructures without Ni detected in EELS spectra. On the other hand, the majority of the EELS measurements showed no traces, within the detection limit, of any oxygen impurities that might have oxidized the iron nanoparticles.

[1] The magic angle was calculated from the Fig. 2 of the article by Jouffrey et al. (2004): for an incident energy of 100 keV, the magic angle value is 2.25 times that of the characteristic scattering angle.

Data analysis

EELS probes unoccupied electron states above the Fermi level in the energy range of core edge levels. This allows measuring the number of scattered electrons of the primary beam which have excited core electrons of the medium to the same interference final state of the X-ray absorption process, assuming that the dipole transition selection rule dominates the matrix element of the scattering process (Kincaid et al. 1978). Within this approximation, EXELFS spectra can be analyzed with the same data procedure as for the EXAFS ones. Therefore, the experimental EXELFS features, i.e., the fine structure which extends for several hundreds of electron volts beyond an inner-shell ionization edge after the excitation of an s (K or L_1) core electron or of $2p$ and $3p$ ($L_{2,3}$ and $M_{2,3}$, respectively) core electrons, are described in terms of a $\chi(k)$ function, also called ionization coefficient (Stern and Rehr 1983), using the EXAFS formula

$$\chi(k) = \sum N_j A_j e^{-2k^2\sigma_j^2} e^{-2R_j/\lambda} \frac{\sin\left[2kR_j + \Phi_j(k)\right]}{kR_j^2}$$

with j being the coordination shell of atoms surrounding the excited atom, and N_j the coordination number of atoms located at an average distance R_j from the central atom. The first exponential term accounts for the motion of atoms due to thermal vibrations and to static disorder. The parameter σ_j is the mean-square relative displacement for the jth shell and the electron wave vector k is related to the emitted electron energy by $k = \sqrt{2m_e(E-E_0)/\hbar^2}$, where E_0 is the edge onset energy, m_e is the electron mass, and $\hbar$ the Planck constant divided by 2π. λ is a phenomenological mean free path that corresponds to a finite lifetime of the excited electron state, $A_j(k, \pi)$ is the backscattering amplitude of the atoms in the jth shell, ϕ_j is the phase shift experienced by the electron on going through the potential of the central and backscattering atoms. In the present paper, we simulated the EXELFS data by using the FEFF8.2 software that calculates the extended X-ray absorption fine structure taking into account the multiple scattering processes (Ankudinov et al. 1998; Ankudinov et al. 2002).

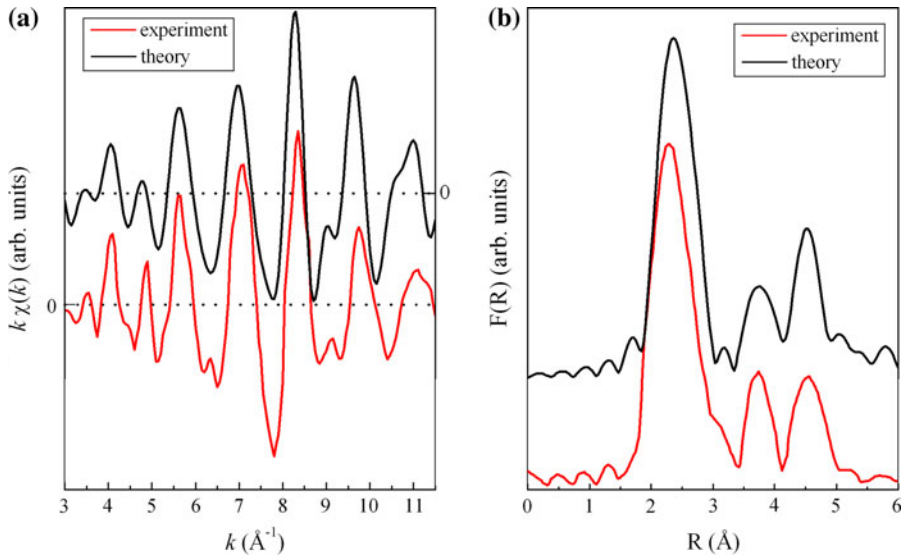

Fig. 1 **a** bcc Fe film $k\chi(k)$ Fe $L_{2,3}$ signals measured through EXAFS (*lower, red line*) and that calculated (*upper, black line*) for Fe bcc lattice with $a = 2.87$ Å considering a cluster of radius $R = 6$ Å, all paths with at least mean amplitude 3.5 % of largest path and a maximum of four scattering atoms. **b** Corresponding Fourier transform obtained for a k-window ranging between 3 and 11.5 Å^{-1}. EXAFS oscillations are adapted with permission from Fig. 2 of Kurde et al. (2007), copyright (2007) by the American Physical Society. (Color figure online)

For the EXELFS simulations, we used the parameters that provided the best fit of the EXAFS spectrum of the Fe bcc film reported in Kurde et al. (2007). Figure 1a shows the experimental EXAFS Fe $L_{2,3}$ signal taken from Kurde et al. (2007) and the one we simulated. The good accordance between the two spectra is clearly visible. This is also highlighted in their corresponding Fourier transform (FT) reported in Fig. 1b. Actually, the Fourier transform of the $k\chi(k)$ oscillations into the real space allows to visually obtain information about the average distance travelled by the electron between the absorbing (ionized, in the EXELFS case) and the various backscattering atoms (shifted by the scattering phase shift). When accounting for only single scattering paths, i.e., paths involving only two scattering atoms, the FT of the EXAFS (EXELFS) oscillations is strictly related to the radial pair distribution functions of each scattering shell. However, even when multiple scattering events are not negligible, at least the first peak of the FT can be associated to the first neighbor atom distance corrected by the phase shift. In particular, starting from a Fe bcc lattice with $a = 2.87$ Å, we found a good reproduction of the experimental data considering a cluster of radius $R = 6$ Å, all paths with at least a mean amplitude 3.5 % of largest path (namely, the one relative to the nearest neighbor atom) and a maximum of four scattering atoms.

Results and discussion

Figure 2 reports the TEM images of three nanoparticles. The lowest panel (Fig. 2a) shows a α-Fe microparticle, while the images in Fig. 2b, c regard two nanoparticles encased in carbon nanotubes. Figure 3 shows the corresponding collected EELS spectral features. The spectra are dominated by two intense and few eV wide peaks due to the transition from the Fe $2p_{3/2,1/2}$ core levels to s and d final unoccupied states. These structures are the so-called white lines corresponding to the L_3 and L_2 edges, respectively. The other features (i.e., oscillations) above 740 eV correspond to the scattering experienced by the $2p_{3/2,1/2}$ electrons in their final unoccupied states. They extend for several hundreds of eV above the edges. As a consequence, the experimental signal is a superposition of the L_3 and L_2 spectra. The L_2 component is shifted in energy with respect to the L_3 one, with an energy separation $\Delta E_{SO} = -13.1$ eV, arising from spin–orbit splitting. Figure 4 shows the corresponding EXELFS signals, $k\chi(k)$, for the three nanoparticles after background subtraction and edge

step normalization of the experimental spectra reported in Fig. 3, over a k range extending up to about 9.0 Å^{-1}. The three oscillatory features present many differences, suggesting that the two iron nanoparticles embedded in the carbon nanotube could not have a bcc structure. Moreover, some differences can be also observed especially at the high oscillation frequency ($k >$ 6 Å^{-1}) between the two EXELFS signals associated to the iron NPs inside the nanotubes. This should mean that the major differences between the two structures involve atoms close to the ionized one. In order to give a closer look at the structure of the nanoparticles, we performed simulations of the EXELFS oscillations starting from known crystallographic lattices. In order to take into account for the presence of the signals due to both the L_3 and L_2 edges, we calculated the total ionization coefficient $\chi(E)$ as following:

$$\chi(E) = 2/3\left(\chi_{L_3}(E) + \alpha\chi_{L_3}(E + \Delta E_{SO})\right)$$

where $\chi_{L_3}(E)$ is the L_3 ionization coefficient and the right part of the equation represents the L_2 one. The intensity ratio, α, between the two signals has been assumed equal to ½, on the basis of 2j + 1 degeneracy in a one-electron model.[2] Figure 5, lower and upper panels, shows the comparison between the experimental and the best simulated $\chi(k)$ oscillations of α-iron microparticle and the NPs encased in the CNT. Their corresponding FTs (i.e., $F(R)$) are also displayed. The k range window used to obtain the Fourier transforms of Fig. 3b extends between 2.5 and 9 Å^{-1} and phase shift corrections have been taken into account. Calculations have been obtained by considering in the former case (lower panel) an iron bcc cluster with lattice parameter $a = 2.87$ Å and in the latter one (upper panel) a Fe fcc structure with a lattice parameter $a = 3.61$ Å. The accordance between the experimental and simulated EXELFS signals is quite good, thus indicating the γ phase of this iron nanoparticle embedded in the carbon nanotube. It is worth noting that the lattice parameter in a fcc Fe lattice has been reported to assume values between 3.4 and 3.7 Å. Therefore, in order to establish the a value that best reproduces the experimental data, we calculated EXELFS spectra considering γ-Fe cluster of atoms with different lattice parameters. The

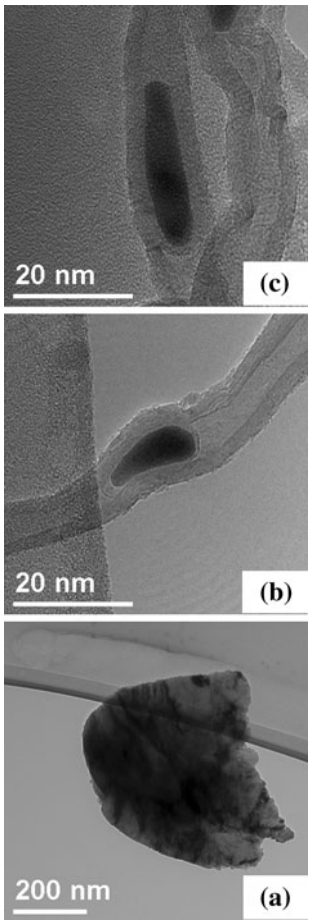

Fig. 2 (*Top to bottom*) TEM images of the two nanoparticles embedded in carbon nanotubes and of a commercial α-Fe microparticle used as standard

accordance between theory and experiment has been quantified by the value of the R factor, defined as the sum of the absolute values of the differences between theory and experiment normalized by the number of experimental points.[3] Figure 6 displays a comparison among the $k\chi(k)$ oscillations calculated for the a values of 3.51 Å (black, left curve), 3.61 Å (red, central curve), and 3.67 Å (green, right curve). The corresponding R values are 0.055, 0.043, and 0.093,

[2] The same approach has been considered for the simulation of the Fe bcc film reported in the "Data analysis" section.

[3] The intensities of the simulated curves have been multiplied by a factor that has been varied between 0.1 and 1 to account a posteriori for an amplitude reduction factor S_0^2, present in the EXELFS formula used by FEFF8.2, not equal to 1. The lowest R factor values were found to occur for S_0^2 equal to 0.25. The R factor values reported in the paper have been obtained for the best S_0^2 value.

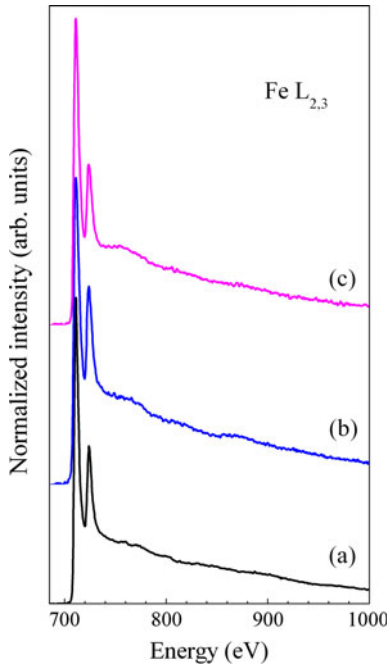

Fig. 3 Near and far $L_{2,3}$ edge energy loss spectra of the three nanoparticles reported in Fig. 2. (*a*), (*b*) and (*c*) curves correspond to the same labelled particles shown in Fig. 1

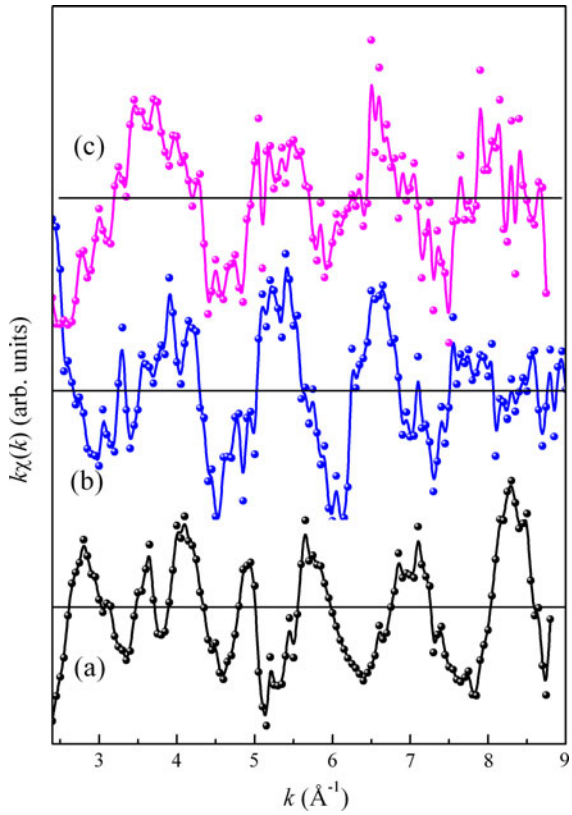

Fig. 4 EXELFS $k\chi(k)$ signals extracted from the experimental spectra reported in Fig. 3, after background subtraction and edge step normalization. (*a*), (*b*) and (*c*) curves correspond to the same labelled particles shown in Fig. 1

respectively. From this result, the obtained lattice parameter of the Fe fcc nanoparticle embedded in the carbon nanotubes is 3.61 ± 0.03 Å. Very interestingly, such a value of the γ-Fe lattice parameter is compatible with a ferromagnetic behavior for the NPs at room temperature with atomic moment higher than that of bulk α-Fe (Zhou et al. 1995). This result confirms the X-ray diffraction analysis performed on a large amount of carbon nanotubes removed from the stainless steel surface reported in Camilli et al. (2012). In addition, our study gives another important piece of information about the structural and dynamical disorder of the nanoparticle, i.e., we can evaluate the Debye–Waller factor, σ^2. In Fig. 7, we display a comparison among the EXELFS oscillations calculated for $\sigma^2 = 0$ (black, dot-dashed curve), 0.004 (red, dashed curve), and 0.008 $Å^2$ (blue, solid curve), showing how much this parameter influences the $k\chi(k)$ fine structure, above all the amplitude of high frequency oscillation. The corresponding *R* factors are 0.069, 0.052, and 0.044, respectively. This result is a little bit higher than the Debye–Waller factor obtained for γ-Fe thin films deposited on copper substrate and analyzed at room temperature (RT) (Butterfield and Crapper 2000). Nonetheless, such finding is absolutely reasonable. In fact, if on one hand the atoms in the NP are compressed by the multiwall CNT, which should lead to a low value of Debye–Waller factor, on the other hand during EXELFS measurements, the system could be at a temperature little bit higher than RT due to the exposure to the high-energetic electron beam, which in turn increases the atomic motion in the NP and thus the Debye–Waller factor's value. As far as the EXELFS features reported in Fig. 3c, we know from X-ray diffraction data reported in Camilli et al. (2012) that iron carbide nanoparticles can be also formed during the carbon nanotube synthesis. Therefore, the cementite theoretical $\chi(k)$ signal was obtained by making a weighted average[4] of the two EXELFS spectra calculated by considering as central

[4] This means that the EXELFS signal calculated for each ionizing Fe atom was weighted for the number of such atoms present in the unit cell.

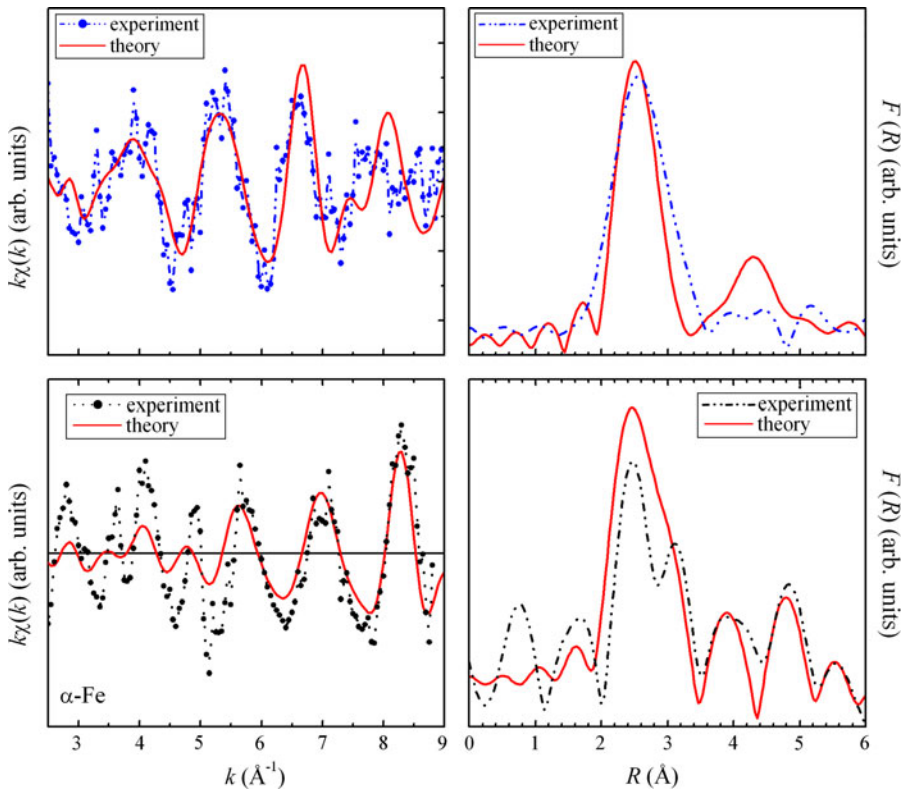

Fig. 5 *Lower panel left*, comparison between the experimental EXELFS oscillations (*black*, *dot–dot dashed*) of the α-Fe microparticle shown in Fig. 2a, and those calculated (*red*, *solid line*) for a bcc lattice with $a = 2.87$ Å. The corresponding Fourier transforms obtained in a k-window of 2.2–9.0 Å^{-1} are reported on the *right*. *Upper panel left*, comparison between the experimental EXELFS oscillations (*black*, *dot–dot dashed*) of the nanoparticle shown in Fig. 2b and those calculated (*red*, *solid line*) for a fcc lattice with $a = 3.60$ Å. The corresponding Fourier transforms obtained in a k-window of 2.2–9.0 Å^{-1} are reported on the *right*. (Color figure online)

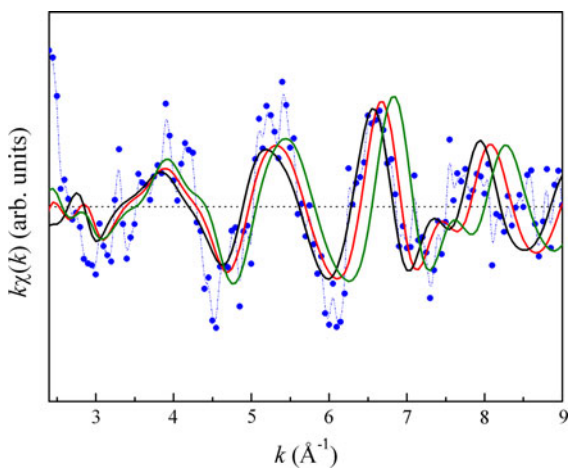

Fig. 6 Comparison among the experimental EXELFS features (*blue*, *dot–dot dashed*) of the nanoparticle shown in Fig. 2b and those calculated for a fcc lattice with $a = 3.51$ Å (*black, left line*), 3.60 Å (*red, central line*), and 3.67 Å (*green, right line*). (Color figure online)

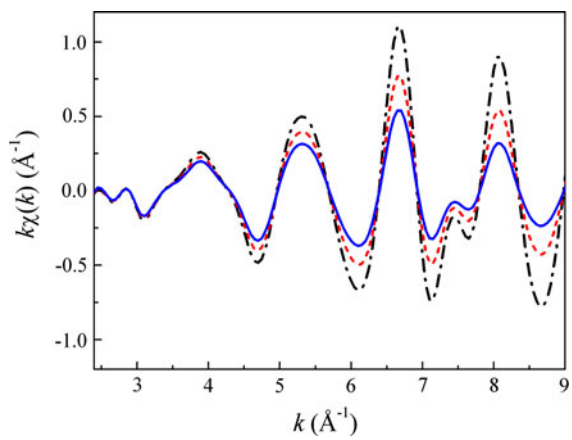

Fig. 7 Comparison among the calculated EXELFS signal for a fcc lattice with $a = 3.60$ Å and $\sigma^2 = 0$ Å^2 (*black*, *dot dashed line*), 0.004 Å^2 (*red*, *dashed line*), and 0.008 Å^2 (*blue*, *solid line*). (Color figure online)

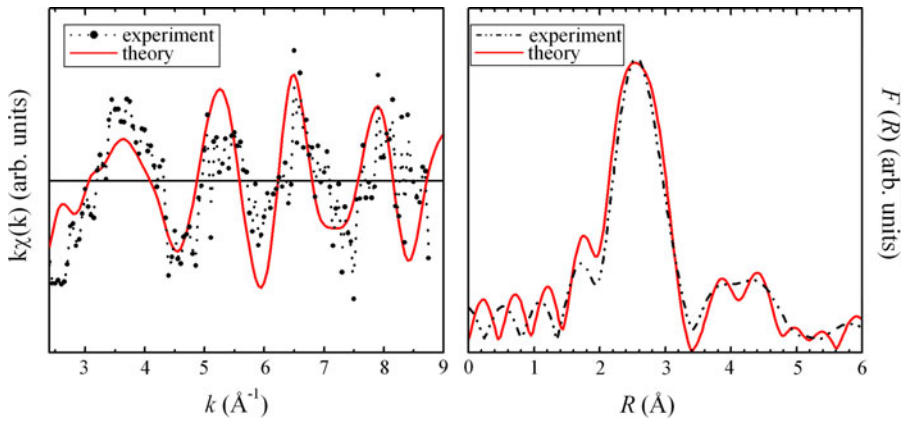

Fig. 8 *Left panel*, comparison between the experimental EXELFS oscillations (*black*, *dot–dot dashed*) of the nanoparticle shown in Fig. 2c and those calculated (*red*, *solid line*) for a Fe_3C lattice. The corresponding Fourier transforms obtained in a *k*-window of 2.2–9.0 Å^{-1} are reported on the *right*. (Color figure online)

atoms the two Fe basis atoms of the Fe_3C unit cell according to the *Pnma* space group symmetry. The lattice parameters used are $a = 5.048$ Å, $b = 6.731$ Å, and $c = 4.513$ Å. In Fig. 8, we report the experimental and simulated $k\chi(k)$ oscillations (left panel) and the corresponding Fourier transforms (right panel). The accordance between theory and experiment is quite good for both the curves, thus evidencing the Fe_3C nature of the nanoparticle.

Conclusions

We performed a detailed structural analysis of the Fe catalytic nanoparticles encapsulated into CNTs directly grown on stainless steel. We demonstrated that EXELFS can be successfully used to obtain information on the local structure around the ionizing atom. In fact, we were able (a) to distinguish between α-Fe, γ-Fe, and iron carbide nanoparticles, (b) to give an estimation of the fcc Fe nanoparticle lattice parameter, which results in being 3.61 ± 0.03 Å. Such a value of the fcc iron lattice parameter suggests that these NPs can be ferromagnetic at room temperature with an atomic moment higher than that of bulk α-Fe.

Acknowledgments This work was supported by the Air Force Office of Scientific Research Material Command, USAF, under grant no. FA8655-11-1-3036.

References

Ankudinov AL, Ravel B, Rehr JJ, Conradson SD (1998) Real-space multiple-scattering calculation and interpretation of X-ray-absorption near-edge structure. Phys Rev B 58:7565

Ankudinov AL, Bouldin CE, Rehr JJ, Sims J, Hung H (2002) Parallel calculation of electron multiple scattering using Lanczos algorithms. Phys Rev B 65:104107

Auerhammer JM, Rez P (1989) Dipole-forbidden excitations in electron-energy-loss spectroscopy. Phys Rev B 40:2024

Bagayoko D, Callaway J (1983) Lattice-parameter dependence of ferromagnetism in bcc and fcc iron. Phys Rev B 28:5419

Borowiak-Palen E, Mendoza E, Bachmatiuk A, Rummeli MH, Gemming T, Nogues J, Skumryev V, Kalenczuk RJ, Pichler T, Silva SRP (2006) Iron filled single-wall carbon nanotubes: a novel ferromagnetic medium. Chem Phys Lett 421:129

Butterfield MT, Crapper MD (2000) Extended X-ray absorption fine structure investigation of the structure of iron overlayers on Cu(111). Surf Sci 454(456):719

Camilli L, Scarselli M, Del Gobbo S, Castrucci P, Nanni F, Gautron E, Lefrant S, De Crescenzi M (2011) The synthesis and characterization of carbon nanotubes grown by chemical vapor deposition using a stainless steel catalyst. Carbon 49:3307

Camilli L, Scarselli M, Del Gobbo S, Castrucci P, Lamastra FR, Nanni F, Gautron E, Lefrant S, D'Orazio F, Lucari F, De Crescenzi M (2012) High coercivity of iron-filled carbon nanotubes synthesized on austenitic stainless steel. Carbon 50:718

Fallon P, Walsh CA (1996) Computer code PEELS. University of Cambridge, England

Gubbiotti G, Albini L, Tacchi S, Carlotti G, Gunnella R, De Crescenzi M (1999) Structural and magnetic properties of epitaxial Cu/Fe/Cu/Si(111) ultrathin films. Phys Rev B 60:17150

He Z, Maurice JL, Gohier A, Lee CS, Pribat D, Cojocaru CS (2011) Iron catalysts for the growth of carbon nanofibers: Fe, Fe_3C or both? Chem Mater 23:5379

Hines WA, Shanthakumar P, Huang T, Budnick JI, Miller RL, Pease DM, Perry DM (2009) Magnetic and structural study of fcc γ -Fe precipitates in Cu. Phys Status Solidi B 246:2154

Jouffrey B, Schattschneider P, Hébert C (2004) The magic angle: a solved mystery. Ultramicroscopy 102:61

Kincaid BM, Meixner AE, Platzman PM (1978) Carbon K edge in graphite measured using electron-energy-loss spectroscopy. Phys Rev Lett 40:1296

Klein J, Campbell SJ, Aubertin F, Gonser U, Schneeweiss O (1991) γ-Fe precipitation in $Cu_{97}Fe_3$ and $Cu_{75}Au_{24}Fe_1$. Phys Status Solidi B 166:87

Kurde J, Ponpandian N, Luo J, Weis C, Baberschke K, Srivastava P, Wende H (2007) Scattering-path analysis and magnetic scattering properties of Fe/Ag(100) films: a temperature-dependent magnetic EXAFS study. Phys Rev B 76:224418

Li DC, Dai L, Huang S, Mau AWH, Wang ZL (2000) Structure and growth of aligned carbon nanotube films by pyrolysis. Chem Phys Lett 316:349

Ling T, Yu H, Liu X, Shen Z, Zhu J (2008) Five-fold twinned nanorods of fcc Fe: synthesis and characterization. Cryst Growth Des 8:4340

Ling T, Zhu J, Yu H, Xie L (2009) Size effect on crystal morphology of faceted face-centered cubic Fe nanoparticles. J Phys Chem C 113:9450

Lyubutin IS, Anosova OA, Frolov KV, Sulyanov SN, Okotrub AV, Kudashov AG, Bulusheva LG (2012) Iron nanoparticles in aligned arrays of pure and nitrogen-doped carbon nanotubes. Carbon 50:2628

Massalski TB, Okamoto H (1992) Binary alloys phase diagrams. ASM International, Materials Park, OH

Mönch I, Leonhardt A, Meye A, Hampel S, Kozhuharova-Koseva R, Elefant D, Wirth MP, Büchner B (2007) Synthesis and characteristics of Fe-filled multi-walled carbon nanotubes for biomedical application. J Phys Conf Series 61:820

Moruzzi VL, Marcus PM, Schwarz K, Mohn P (1986) Ferromagnetic phases of bcc and fcc Fe, Co, and Ni. Phys Rev B 34:1784

Shen J, Ohresser PCh, Klaua M, Barthel J, Kirschner J (1998) Magnetic moment of fcc Fe(111) ultrathin films by ultrafast deposition on Cu(111). Phys Rev Lett 80:1980

Stern EA, Rehr JJ (1983) Many-body aspects of the near-edge structure in X-ray absorption. Phys Rev B 27:3351

Stöhr J (1988) X-ray absorption: principles, applications, techniques of EXAFS, SEXAFS and XANES. In: Koningsberger DC, Prins R (eds) Chemical analysis: a series of monographs on analytical chemistry, vol 92. Wiley, New York, p 443

Winkler A, Mühl T, Menzel S, Koseva RK, Hampel S, Leonhardt A, Büchner B (2006) Magnetic force microscopy sensors using iron-filled carbon nanotubes. J Appl Phys 99:104905

Zhou YM, Zhang WQ, Zhong LP, Wang DS (1995) Theoretical prediction of ferrimagnetism in face-centered cubic iron. J Magn Magn Mater 145:L273